Phasor Correction of Coupling Capacitor Voltage Transformers for High-Performance Protection

Eubis Pereira Machado, Damásio Fernandes Júnior, Washington Luiz Araújo Neves

***Abstract*—The algorithms for the correction of transients in coupling capacitor voltage transformers (CCVTs) are generally designed from processing samples in the time domain. Therefore, they need to be embedded in the measurement, protection, and control devices, because in these instruments only the phasors are available for the development of dedicated applications. In this paper, as an extension of a method originally developed by these authors for the time domain correction of CCVT secondary voltage samples, a mathematical formulation is developed that demonstrates the applicability of the existing method for phasor compensation, regardless of the phasor estimation algorithm used. Three phasor estimation algorithms and two CCVTs with different topologies and voltage levels are used to evaluate the method's performance. ATP (Alternative Transients Program) was used to generate the oscillographic records, while the phasor estimation algorithms and their corrections were implemented in MatLab. From the results, it can be inferred that the evaluated method can be used to correct voltage phasor disturbances, providing more suitable signals for protection algorithms.**

***Keywords*—Digital filter, instrument transformer, intelligent electronic device, phasor estimation, phasor measurement unit.**

I. Introduction

CCVTs are essential equipment for high, extra-high, and ultra-high voltage substations, given their technical and economical measurement characteristics. However, during a surge of the primary voltage, the equipment may develop a transient response that affects the performance of the distance relays [1]–[6] and phasor measurements unit (PMU) [7], [8], because these devices use phasor estimation algorithms, whose accuracy and convergence speed depend on the frequency of the CCVT secondary voltage waveform.

Phasor estimation algorithms have been a constantly evolving area of study [9]–[11]. In general, most of the new propositions are based on modifications of the discrete Fourier transform (DFT) and seek to improve the performance of the phasors of current signals given the presence of the unidirectional component of the short-circuit current and the saturation of current transformers [12]–[14]. Nevertheless, due to the difficulty in eliminating spurious components from the CCVT transient response, some phase estimation algorithms have been improved for this purpose [15]–[17]. Although they perform well, they are formulated according to a specific CCVT topology, require knowledge of the model parameters and require a sampling rate higher than 64 samples per cycle of the power frequency. Moreover, because they are new phasor estimation algorithms, they need knowledge of samples in the time domain, so they must be embedded in the intelligent electronic device (IED) and PMU during the manufacturing process.

Different strategies have been devised to perform the correction of the CCVT secondary voltage in the time domain. Although they perform well, the techniques require knowledge of the operating equipment model and its parameters [18]–[25] and some of them can be used only in dedicated applications, given the dependence on the dynamic characteristics of the power system used [20]–[23]. Recently, some correction methods have been developed to be independent of the CCVTs model, the determination of its parameters, as well as the investigated power system [6], [26]. Using only the frequency response between 10 and 60 Hz, [6] developed a digital filter that corrects samples in the time domain of the secondary voltage. In [26], using a mathematical model for the transient response as well as samples of the secondary voltage during the first fault cycle, the authors used frequency modulation and Prony concepts to identify the parameters of the mathematical model of the secondary voltage to correct the current voltage reading. Although it has the advantage of CCVT model independence, the methodology developed by [26] requires a high sampling rate (256 samples per cycle), requires a considerable computational effort for real-time parameter identification, and requires a one-cycle delay of the fundamental to initialize its actuation. Furthermore, in the current state of IED and PMU manufacturing, the aforementioned correction techniques can only be incorporated during the device manufacturing process, or need to be implemented in a dedicated device such as a digital signal processor (DSP), since users are not allowed to incorporate digital filters before the phasor estimation process. Therefore, the development of a phasor correction technique is critical for commercial device applications.

In this work, the methodology developed in [6] will be extended for processing signals represented in the frequency domain, in order to allow the dynamic correction of the secondary voltage phasors, regardless of the algorithm used by IEDs and PMUs. Like its time domain version, the methodology does not depend on the structure of the power system or the CCVT model and the identification of its parameters, since only the frequency response of the equipment under analysis is required. In order to verify

E. P. Machado is with Collegiate of Electrical Engineering, Federal University of Vale do São Francisco, Av. Antônio Carlos Magalhães, 510, Santo Antônio, Juazeiro-BA 48.902-300, Brazil (e-mail: eubis.machado@univasf.edu.br).

D. Fernandes Jr. and W. L. A. Neves are with Department of Electrical Engineering at Federal University of Campina Grande, 882 Aprígio Veloso Av, Bodocongó, Campina Grande-PB 58.429-140, Brazil. (e-mail: damasio@dee.ufcg.edu.br., waneves@dee.ufcg.edu.br.

Paper submitted to the International Conference on Power Systems Transients (IPST2023) in Thessaloniki, Greece, June 12-15, 2023.

the effectiveness of the developed formulation, four CCVT models reported in the literature were used, namely: 138 kV [27], 230 kV [28], 230 kV [29] and 500 kV [30], as well as different phasor estimation techniques, namely: full-cycle DFT (FCDFT) [31], cosine filter (CF) [32] and modified cosine filter (MCF) [33]. The ATP was used to simulate the power system and instrument transformers, while the basic architecture of the IED and PMU containing the anti-aliasing filtering, sampling, phasor estimation algorithms, and their corrections were implemented in MatLab. Gain and phase estimation errors, as well as distance protection performance analyses, are used to quantify the impact of dynamic voltage phasor correction.

II. DFT-Based Phasor Estimation Techniques

DFT-based phasor estimation algorithms use samples of one, half, or fractions of the cycle of a sequence $x(n)$ to extract the fundamental component of the signal. Three full-cycle algorithms are presented below.

A. Full-cycle DFT

In the conventional FCDFT algorithm, the real and imaginary phase quantities of the fundamental component of $x(n)$ can be obtained, respectively, by (1) [31]:

$$\begin{aligned} X_{c1} &= \frac{2}{N}\sum_{n=0}^{N-1} x(n)\cos\left(\frac{2\pi n}{N}\right) \\ X_{s1} &= -\frac{2}{N}\sum_{n=0}^{N-1} x(n)\sin\left(\frac{2\pi n}{N}\right) \end{aligned} \tag{1}$$

The formulation presented in (1) is not convenient for computational implementation, since they contemplate a fixed window of N samples of $x(n)$. Making use of the concept of convolution sum [34], one can infer that the real and imaginary parts of the fundamental component of $x(n)$, when the k-th sample of $x(n)$ is being processed are represented, respectively, by (2).

$$\begin{aligned} X_{c1}(k) &= \sum_{n=0}^{N-1} x(k-n)h_{c1}(n) \\ X_{s1}(k) &= \sum_{n=0}^{N-1} x(k-n)h_{s1}(n) \end{aligned} \tag{2}$$

Where,

$$\begin{aligned} h_c(n) &= \frac{2}{N}\left[\cos\left(2\pi\frac{1}{N}\right)\ \ldots\ \cos\left(2\pi\frac{N-1}{N}\right)\ \cos(2\pi)\right] \\ h_s(n) &= \frac{2}{N}\left[\sin\left(2\pi\frac{1}{N}\right)\ \ldots\ \sin\left(2\pi\frac{N-1}{N}\right)\ \sin(2\pi)\right] \end{aligned} \tag{3}$$

Once the real and imaginary components are known, the amplitude and phase of the phasors can be computed by (4).

$$\begin{aligned} |\widehat{X}_1(k)| &= \sqrt{X_{c1}^2(k) + X_{s1}^2(k)} \\ \phi_1(k) &= tg^{-1}\left(\frac{X_{s1}(k)}{X_{c1}(k)}\right) \end{aligned} \tag{4}$$

B. Cosine Filter

Due to the better elimination characteristics of the exponential decay DC component, the h_{c1} (CF) filter can be used to extract the real and imaginary parts of the phasors [32]. However, to promote the orthogonality observed in the h_{c1} and h_{s1} filters, the data window for extracting the imaginary component needs to be shifted by a quarter cycle. From [32], it can be inferred that the real and imaginary parts of the phasors can be expressed by (5).

$$\begin{aligned} X_{c2}(k) &= X_{c1}(k) \\ X_{s2}(k) &= \sum_{n=0}^{N-1} x(k-n-\frac{N}{4})h_{c1}(n) \end{aligned} \tag{5}$$

C. Modified Cosine Filter

The CF formulation has the disadvantage of requiring a quarter-cycle delay concerning FCDFT. Hence, a new formulation for computing $X_{s2}(k)$ called MCF was presented in [33]. In it, the data window is delayed by only one sample, as shown in (6).

$$X_{s3}(k) = \sum_{n=0}^{N-1}\left[x\left(k-n-1\right) - x(k-n)\cos(\alpha)\right]\frac{h_{c1}(n)}{\sin(\alpha)} \tag{6}$$

Where α is the angle difference between two consecutive samples, therefore, expressed by $\frac{2\pi}{N}$.

III. Proposed technique

The correction of CCVT transients has delivered improvements in the safety, reliability, and speed of distance protection, as well as assisting controlled switching algorithms for transmission lines with shunt [35] and series compensation [36]. However, the digital filters are designed to process samples in the time domain, therefore requiring a device for dedicated or needing to be embedded in IEDs and PMUs during their manufacture. Motivated by the current technology of these devices, in which the phasors are available for processing, this section extends the methodology proposed by [6], in the sense of demonstrating that the recursive digital filter (RDF) used to correct time-domain samples of the CCVT secondary voltage can also be employed to correct the phasors obtained from secondary voltage samples, regardless of the phasor estimation algorithms.

According to [6], only using the CCVT frequency response information between 10 and 60 Hz, the RDF expressed by (7) corrects the low-frequency transients of the equipment, regardless of its model and operating characteristics of the power system.

$$H_d(z) = \frac{Y(z)}{X(z)} = k_0\prod_{i=1}^{p}\frac{1 + c_{i1}z^{-1} + c_{i2}z^{-2}}{1 + d_{i1}z^{-1} + d_{i2}z^{-2}} \tag{7}$$

Where p is the number of second-order sections, c_i and d_i ($i = 1,\ldots,p$) are the RDF coefficients and k_0 is a scaling constant, which are obtained through a multi-objective optimization method. The $X(z)$ and $Y(z)$ signals correspond to the discrete frequency domain representation of the input and output RDF signal, respectively.

Because it allows a better mathematical treatment, the second-order cascade structure expressed in (7) will be replaced by the direct form given by (8).

$$\frac{Y(z)}{X(z)} = \frac{\sum_{i=0}^{gn} a_i z^{-i}}{1 + \sum_{i=1}^{gd} b_i z^{-i}} \tag{8}$$

Where gn and gd are the order of the polynomial of the numerator and denominator of $H_d(z)$, respectively.

Applying the inverse z transform to (8) gives the difference equation represented by (9).

$$y(k) = \sum_{i=0}^{gn} a_i x(k-i) - \sum_{i=1}^{gd} b_i y(k-i) \tag{9}$$

Where $x\,(k-i)$ and $y\,(k-i)$ are the $i-$th time sample of the CCVT secondary voltage and its sample corrected, respectively.

Let $h_{\text{Re}}(n)$ and $h_{\text{Im}}(n)$ become digital filters responsible for extracting the real and imaginary component, respectively, of the phasor $\widehat{Y}(k)$ of a sequence $y(k)$. Therefore, the real and imaginary components of $\widehat{Y}(k)$ can be calculated by (10), being m the length of the digital filters.

$$\begin{aligned} Y_{\text{Re}}(k) &= \sum_{n=0}^{m} y(k-n) h_{\text{Re}}(n) \\ Y_{\text{Im}}(k) &= \sum_{n=0}^{m} y(k-n) h_{\text{Im}}(n) \end{aligned} \tag{10}$$

Substituting (9) into (10), gives:

$$\begin{aligned} Y_{\text{Re}}(k) = &\sum_{n=0}^{m} \sum_{i=0}^{gn} a_i x\left[(k-i)-n\right] h_{\text{Re}}(n) \\ &- \sum_{n=0}^{m} \sum_{i=1}^{gd} b_i y\left[(k-i)-n\right] h_{\text{Re}}(n) \end{aligned} \tag{11}$$

$$\begin{aligned} Y_{\text{Im}}(k) = &\sum_{n=0}^{m} \sum_{i=0}^{gn} a_i x\left[(k-i)-n\right] h_{\text{Im}}(n) \\ &- \sum_{n=0}^{m} \sum_{i=1}^{gd} b_i y\left[(k-i)-n\right] h_{\text{Im}}(n) \end{aligned} \tag{12}$$

Alternating the order of operation of the summations in (11) and (12) gives (13) and (14), respectively.

$$\begin{aligned} Y_{\text{Re}}(k) = &\sum_{i=0}^{gn} a_i \sum_{n=0}^{m} x\left[(k-i)-n\right] h_{\text{Re}}(n) \\ &- \sum_{i=1}^{gd} b_i \sum_{n=0}^{m} y\left[(k-i)-n\right] h_{\text{Re}}(n) \end{aligned} \tag{13}$$

$$\begin{aligned} Y_{\text{Im}}(k) = &\sum_{i=0}^{gn} a_i \sum_{n=0}^{m} x\left[(k-i)-n\right] h_{\text{Im}}(n) \\ &- \sum_{i=1}^{gd} b_i \sum_{n=0}^{m} y\left[(k-i)-n\right] h_{\text{Im}}(n) \end{aligned} \tag{14}$$

From (13) and (14), one can infer that $h_{\text{Re}}(n)$ and $h_{\text{Im}}(n)$ operate on the m samples of $x\left[(k-i)-n\right]$ and $y\left[(k-i)-n\right]$, therefore allowing one to write according to (15).

$$\begin{aligned} Y_{\text{Re}}(k) &= \sum_{i=0}^{gn} a_i X_{\text{Re}}(k-i) - \sum_{i=1}^{gd} b_i Y_{\text{Re}}(k-i) \\ Y_{\text{Im}}(k) &= \sum_{i=0}^{gn} a_i X_{\text{Im}}(k-i) - \sum_{i=1}^{gd} b_i Y_{\text{Im}}(k-i) \end{aligned} \tag{15}$$

Where $X_{\text{Re}}(k-i)$, $X_{\text{Im}}(k-i)$, $Y_{\text{Re}}(k-i)$, $Y_{\text{Im}}(k-i)$ are the $i-$th preceding samples of the real and imaginary part of the phasors $\widehat{X}(k)$ and $\widehat{Y}(k)$, respectively.

As the corrected phasor can be expressed in the form of (16)

$$\widehat{Y}(k) = Y_{\text{Re}}(k) + jY_{\text{Im}}(k) \tag{16}$$

Replacing (15) with (16), it is possible to express (17).

$$\begin{aligned} \widehat{Y}(k) = &\left[\sum_{i=0}^{gn} a_i X_{\text{Re}}(k-i) - \sum_{i=1}^{gd} b_i Y_{\text{Re}}(k-i)\right] \\ &+ j\left[\sum_{i=0}^{gn} a_i X_{\text{Im}}(k-i) - \sum_{i=1}^{gd} b_i Y_{\text{Im}}(k-i)\right] \\ = &\sum_{i=0}^{gn} a_i \widehat{X}(k-i) - \sum_{i=1}^{gd} b_i \widehat{Y}(k-i) \end{aligned} \tag{17}$$

Where,

$$\begin{aligned} \widehat{X}(k-i) &= X_{\text{Re}}(k-i) + jX_{\text{Im}}(k-i) \\ \widehat{Y}(k-i) &= Y_{\text{Re}}(k-i) + jY_{\text{Im}}(k-i) \end{aligned} \tag{18}$$

is the $i-$th sample of the phasors estimated by IED or PMU and corrected by RDF, respectively.

From (17), it can be inferred that the effectiveness of the correction of the secondary voltage phasors of a CCVT requires only the last gn samples of the $\widehat{X}(k)$ phasor and the last gd samples of $\widehat{Y}(k)$. Note that, unlike traditional filtering methods where the input and output sequences belong to the set of real numbers, in (17) the sequences $\widehat{X}(k)$ and $\widehat{Y}(k)$ belong to the set of complex numbers. For completeness of the analysis, transforming (17) to z domain results in (19), whose representation in cascade form is given by (20).

$$\frac{\mathcal{Z}\{\widehat{Y}(k)\}}{\mathcal{Z}\{\widehat{X}(k)\}} = \frac{\sum_{i=0}^{gn} a_i z^{-1}}{1 + \sum_{i=1}^{gd} b_i z^{-1}} \tag{19}$$

$$= k_0 \prod_{i=1}^{p} \frac{1 + c_{i1} z^{-1} + c_{i2} z^{-2}}{1 + d_{i1} z^{-1} + d_{i2} z^{-2}} \tag{20}$$

Where, $\mathcal{Z}\{\cdot\}$ is the z transform operator. By inspection of (7) and (20), it can be inferred that the digital filters used for sample correction of the secondary voltage of a CCVT can also be used for sample correction of the respective voltage phasor which is merely a complex sequence.

IV. Evaluation of the Dynamic Phasor Correction

Different models of CCVTs have been reported in the literature. In this work, to validate the performance of the method under investigation, the models presented in Fig. 1

were used, whose nonlinear characteristic of the magnetic core of the inductive potential transformer of the 230 kV CCVT (Passoni-Villa) is shown in Table I [28].

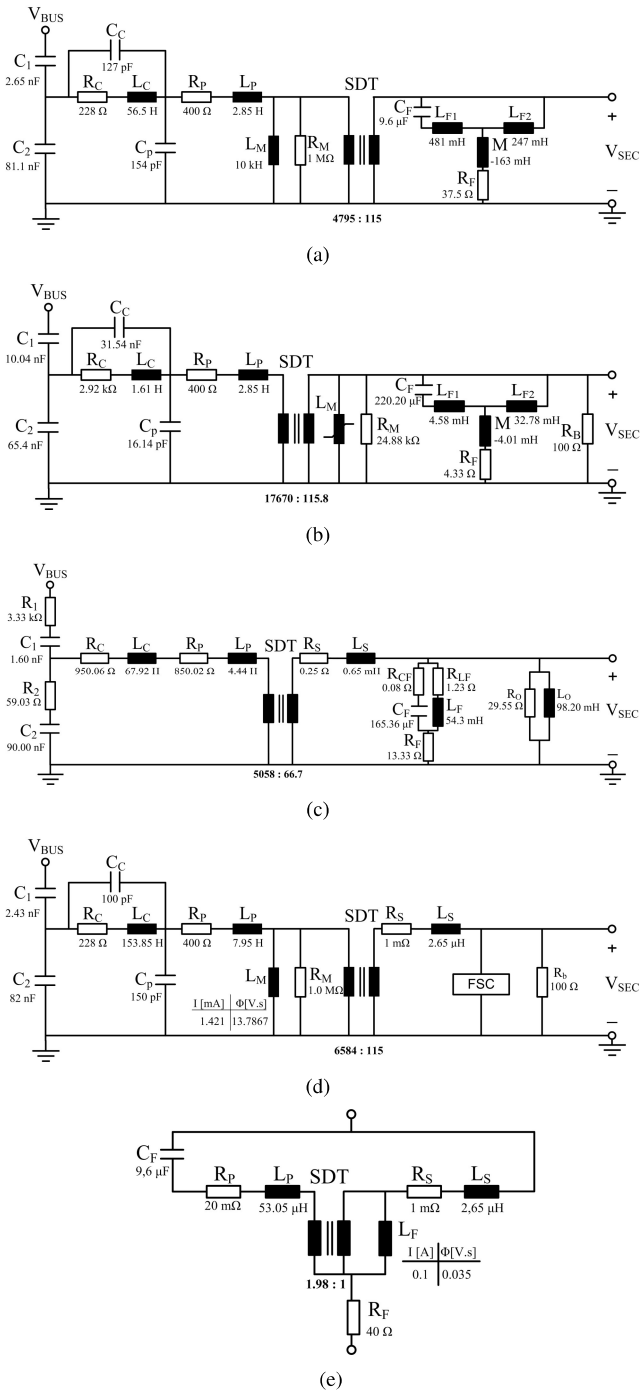

Fig. 1. CCVT models and its parameters. (a) 138 kV CCVT model proposed by [27] (type PCA-8 manufactured by Westinghouse). (b) 230 kV CCVT model adapted from [28] (type 245/8M manufactured by Passoni-Villa). (c) 500 kV CCVT model proposed by [30]. (d) 230 kV CCVT model proposed by [29] and (e) Its Ferroresonance Suppression Circuit (FSC).

Assuming a sudden sag in the voltage V_{BUS}, a simplification used to set up a fault in the power system, Fig. 2 shows a typical behavior of the normalized secondary voltage of the CCVTs. The signals have similar dynamics, but the 500 kV device has a higher overshoot and time constant. Because

TABLE I
NONLINEAR CHARACTERISTIC OF THE POTENTIAL TRANSFORMER MAGNETIC CORE OF THE 230 KV CCVT (PASSONI-VILLA).

Current (A)	Flux (V s)
0.076368	0.025772
0.720881	0.189066
1.429369	0.396889
2.511675	0.748388
3.662012	0.863553
4.587227	0.903317
5.712037	0.942706
55.527018	1.556415
5552.7018	1.562242

they present frequency components of difficult rejection, the performance of phasor estimation algorithms can be affected, justifying the development of recent time domain correction methodologies [10], [25].

In this work, in a novel way, the subsidence transients are corrected after the phasor estimation process, according to (17), whose coefficients c_i and d_i of the equivalent cascade form are obtained from the gain and phase frequency responses of the relationship $\frac{V_{\mathrm{SEC}}(j\omega)}{V_{\mathrm{BUS}}(j\omega)}$ shown in Fig. 3(a) and 3(b), respectively. Note that these devices exhibit similar characteristics for frequencies below 60 Hz, which are defined by a resonant peak and low-frequency attenuation.

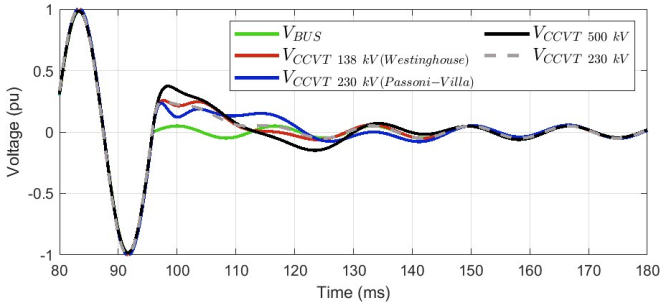

Fig. 2. Subsidence transients of the four CCVTs analyzed.

Using the CCVTs frequency response for $2\pi \cdot 10 \leq \omega \leq 2\pi \cdot 60$ rad/s and the digital filter design methodology presented in [6], the RDF coefficients of the four CCVTs are shown in Table II, considering a sampling rate of 32 samples per cycle of the power frequency. To quantify the impact of using the proposed phasor correction method, the amplitude relative error (ARE) and the phase absolute error (PAE) were used, as follows (21).

$$\begin{aligned} \mathrm{ARE} &= \frac{\left|\widehat{X}_{\mathrm{ref}}(k)\right| - \left|\widehat{X}_{\mathrm{est}}(k)\right|}{\left|\widehat{X}_{\mathrm{ref}}(k)\right|} \\ \mathrm{PAE} &= \angle\widehat{X}_{\mathrm{ref}}(k) - \angle\widehat{X}_{\mathrm{est}}(k) \end{aligned} \tag{21}$$

Where,

- $\widehat{X}_{\mathrm{ref}}(k)$ is the $\widehat{V}_{\mathrm{BUS}}$ phasor referenced to the CCVT secondary side;
- $\widehat{X}_{\mathrm{est}}(k)$ is the $\widehat{V}_{\mathrm{SEC}}$ phasor or its RDF-compensated.

In Figs. 4 and 5 are shown, respectively, the ARE and PAE of all investigated CCVTs, when using the FCDFT,

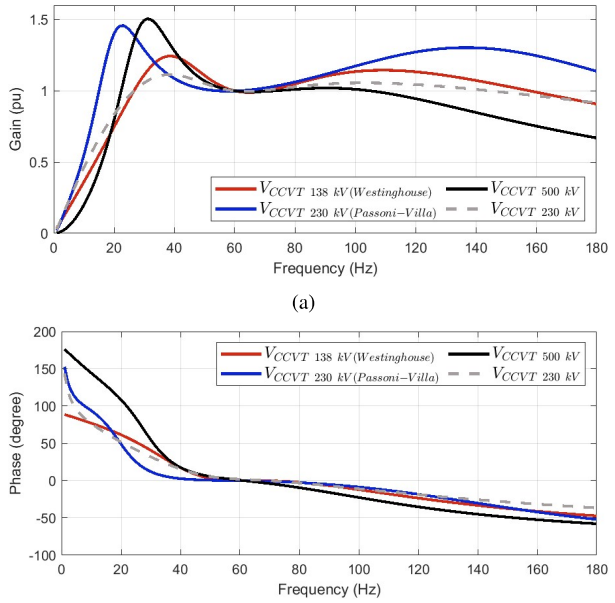

Fig. 3. Frequency response of the CCVTs: (a) Gain. (b) Phase.

TABLE II
RECURSIVE DIGITAL FILTERS PARAMETERS

	RDF parameters of the 138 kV CCVT (Westinghouse type PCA-8)				
Section i	c_{i1}	c_{i2}	d_{i1}	d_{i2}	$k_0 = 4.2551$
1	-1.5540	0.6427	-1.8119	0.8475	—
2	-1.8636	0.8807	-0.0198	-0.9801	—
	RDF parameters of the 230 kV CCVT (Passoni-Villa type 245/8M)				
Section i	c_{i1}	c_{i2}	d_{i1}	d_{i2}	$k_0 = 3.6475$
1	$-1,4315$	$0,6465$	$-1,9998$	$0,9998$	—
2	$-1,9417$	$0,9462$	0	0	—
3	$-1,5087$	$0,5121$	$-1,6526$	$0,6774$	—
	RDF parameters of the 230 kV CCVT				
Section i	c_{i1}	c_{i2}	d_{i1}	d_{i2}	$k_0 = 4.2277$
1	-1.4369	0.6315	0.2493	-0.7093	—
2	-1.9418	0.9463	-1.8955	0.8960	—
3	-1.9874	0.9875	-1.9977	0.9977	—
	RDF parameters of the 500 kV CCVT				
Section i	c_{i1}	c_{i2}	d_{i1}	d_{i2}	$k_0 = 6.2188$
1	-1.5847	0.6765	-1.7525	0.7814	—
2	-1.9281	0.9373	0.0591	-0.9409	—
3	-1.8839	0.8873	-1.9996	0.9996	—

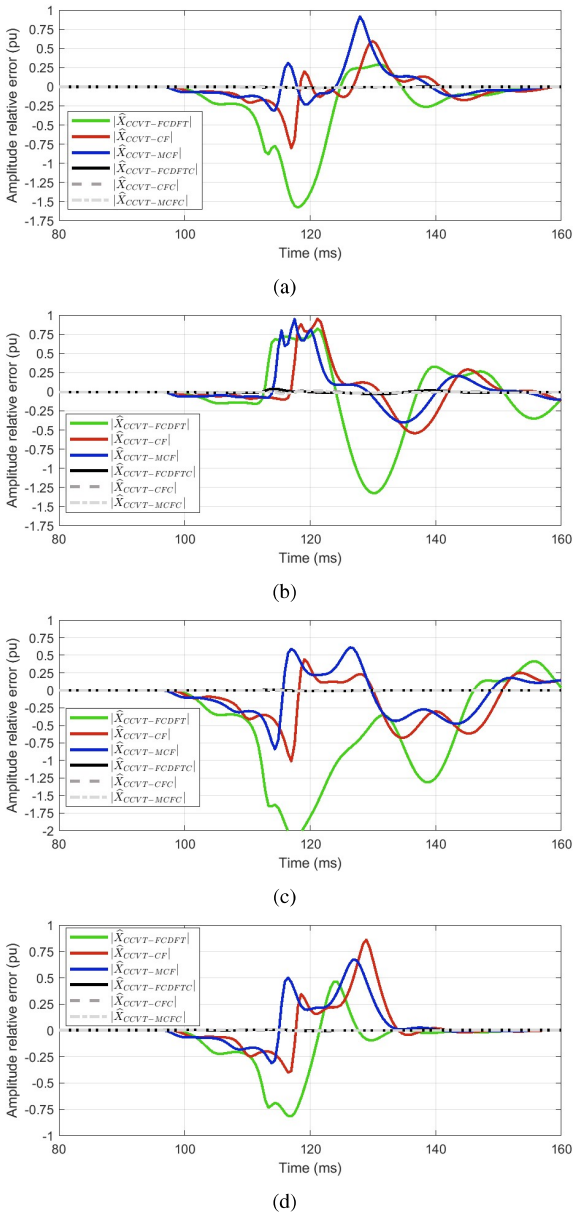

Fig. 4. Amplitude relative error: (a) 138 kV CCVT (Westinghouse). (b) 230 kV CCVT (Passoni-Villa). (c) 500 kV CCVT. (d) 230 kV CCVT.

CF and MCF phasor estimation algorithms, as well as the RDF-corrected algorithms, denoted in this paper as FCDFTC (FCDFT corrected), CFC (CF corrected) and MCFC (MCF corrected). Corroborating with the input signals displayed in Fig. 2, it can be seen that the 500 kV CCVT causes larger amplitude errors and with longer duration time, regardless of the phasor estimation algorithm used.

From the results shown in Figs. 4 and 5, it can be seen that CCVT subsidence transients cause severe errors during the estimation of the amplitude and phase of the phasors, suggesting that the algorithms used in commercial IEDs may not perform well during those transients. For the three algorithms evaluated, the results prove that the use of RDF initially developed for corrections of secondary voltage samples in the time domain operates successfully in the correction of secondary voltage phasors, providing more assertive estimates for the protection and control algorithms.

In order to quantify the errors in estimating the amplitude and phase of the phasors during transient operating conditions, based on the dynamics shown in Figs. 4 and 5, a window in the range 100 ms $\leq t_{w1} \leq$ 160 ms (3.6 cycles) was used for the 500 kV and 230 kV (Passoni-Villa) CCVTs, while for the 138 kV (Westinghouse) and 230 kV CCVTs the 100 ms $\leq t_{w2} \leq$ 140 ms (2.4 cycles) window was used. For the informed windows, the Table III shows the mean absolute percentage error (MAPE) of the amplitude, as well as the root mean square error (RMSE) of the phase of the CCVT secondary voltage phasors. These error metrics are calculated

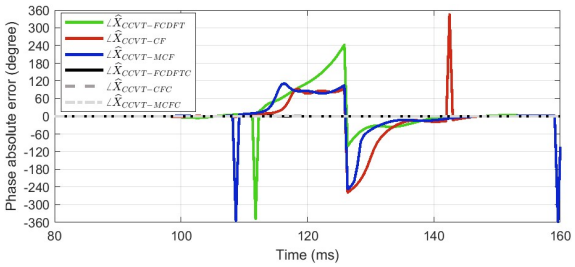

(a)

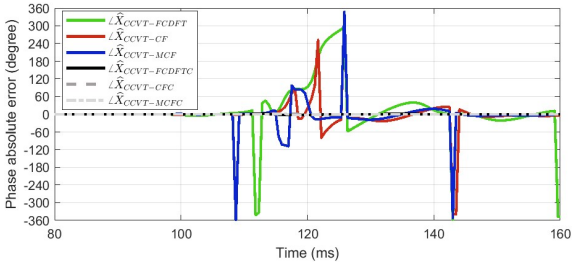

(b)

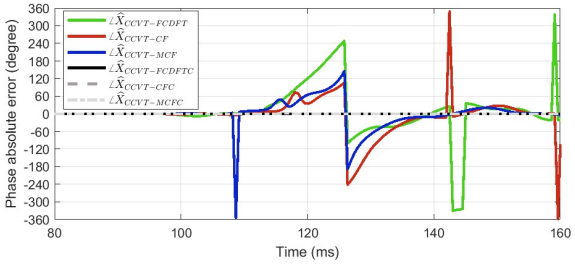

(c)

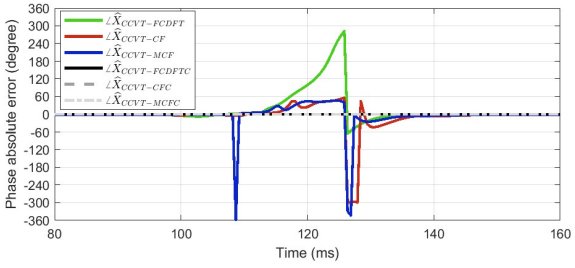

(d)

Fig. 5. Phase absolute error: (a) 138 kV CCVT (Westinghouse). (b) 230 kV CCVT (Passoni-Villa). (c) 500 kV CCVT. (d) 230 kV CCVT.

according to (22).

$$\text{MAPE} = \frac{1}{n}\sum_{k=i}^{npt_j}\left|\frac{\left|\widehat{X}_{\text{ref}}(k)\right| - \left|\widehat{X}_{\text{est}}(k)\right|}{\left|\widehat{X}_{\text{ref}}(k)\right|}\right| \cdot 100$$
$$\text{RMSE} = \sqrt{\frac{1}{n}\sum_{k=i}^{npt_j}\left(\angle\widehat{X}_{\text{ref}}(k) - \angle\widehat{X}_{\text{est}}(k)\right)^2} \quad (22)$$

Where $npt_j = \frac{t_{wj}}{60 \cdot N}$, for $j \in \{1,\ 2\}$.

From the error results shown in Table III, it can be seen that the largest amplitude and phase errors were observed in FCDFT, followed by CF and MCF, respectively. Regardless of the topology of the CCVTs and the phasor estimation algorithm, it can be inferred that RDF provides amplitude and phase correction, with the largest errors recorded

TABLE III
ERRORS OF THE CCVTS SECONDARY VOLTAGE PHASORS

	138 kV CCVT (Westinghouse)		230 kV CCVT (Passoni-Villa)	
Algorithm	MAPE (%)	RMSE (degree)	MAPE (%)	RMSE (degree)
FCDFT	45.98	88.54	40.97	97.28
CF	18.57	83.54	20.19	63.76
MCF	19.64	82.32	18.19	63.19
FCDFTM	0.58	0.35	1.29	0.95
CFM	0.57	0.33	0.93	0.54
MCFM	0.60	0.01	0.90	0.01
	500 kV CCVT		230 kV CCVT	
Algorithm	MAPE (%)	RMSE (degree)	MAPE (%)	RMSE (degree)
FCDFT	73.16	97.81	24.95	80.28
CF	30.90	68.83	21.45	72.13
MCF	29.12	58.71	20.82	71.44
FCDFTM	0.24	0.15	0.27	0.12
CFM	0.19	0.17	0.23	0.15
MCFM	0.25	0.01	0.26	0.00

corresponding to 1.29% for amplitude and 0.95 degree for phase. In general, the errors in the amplitude of the phasors can be associated with the phenomena of underreach, overreach, and velocity operation of the distance protection, while the phase errors can be related to the loss of directionality of the protection. Therefore, the phasor corrections performed by RDF can improve the reliability, security, and velocity for high-performance phasor-based protection.

A. Distance Protection Performance Analysis

To quantify the impact of the correction of the secondary voltage phasors of the CCVTs on the distance protection performance, the 230 kV power system shown in Fig. 6 was implemented in the ATP software. The transmission lines have a length of 80 km and parameters shown in Table IV. The Thévenin equivalents data are presented in Table V, the ideal current transformers (CT) ratio is 100:5, while the 230 kV CCVTs were represented by the model shown in Figs. 1(d) and 1(e). In the system regions represented by $d_1 \in \{0.1,\ 0.2,\ \ldots,\ 0.8\}$ pu and $d_2 \in \{0.05,\ 0.1,\ 0.015,\ 0.2\}$ pu, faults of the single line-to-ground (L-G), line-to-line (L-L), double line-to-ground (L-L-G) and symmetrical fault (L-L-L) types were simulated for $L \in \{A,\ B,\ C\}$ with different incidence angles $\delta \in \{0,\ 30°,\ 60°,\ 90°\}$ and a fault resistance of 1.0 Ω. The oscillographic records of the fault events were processed by a distance relay implemented in MatLab software, adopting a range of 80% for the first zone, the conventional FCDFT algorithm, and the mho characteristic with different types of polarization, namely self-polarized, cross-polarized, and memory-polarized, were adopted.

TABLE IV
TRANSMISSION LINES PARAMETERS

Sequence	$R(\Omega/km)$	$X(\Omega/km)$	$\omega C(\mu\mho/km)$
Zero	0.4366	1.5034	3.3489
Positive	0.0494	0.2750	6.2656

Processing the oscillograph records for faults in the d_1 region, when performing the correction of the secondary voltage phasors of the CCVTs, the reductions in fault detection

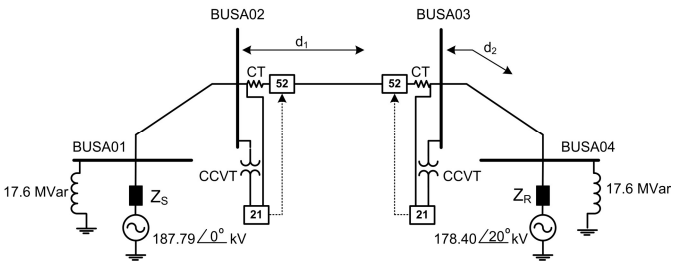

Fig. 6. Electric power system used for distance protection analysis.

TABLE V
PARAMETERS OF THE THÉVENIN EQUIVALENTS

	Zero sequence		Positive sequence	
Impedance	$R_0(\Omega)$	$X_0(\Omega)$	$R_1(\Omega)$	$X_1(\Omega)$
Z_S	7.7900	220.9400	0.4100	198.0000
Z_R	1.1268	66.8400	0.9681	44.0000

time by the protection unit installed at BUSA02 are presented in Fig. 7. The results show that the reduction in fault detection time (RFDT) is a function of the type of polarization used by the mho, reaching values corresponding to one cycle of the fundamental with the mho self-polarized and 3.5 ms with the cross- or memory-polarized ones.

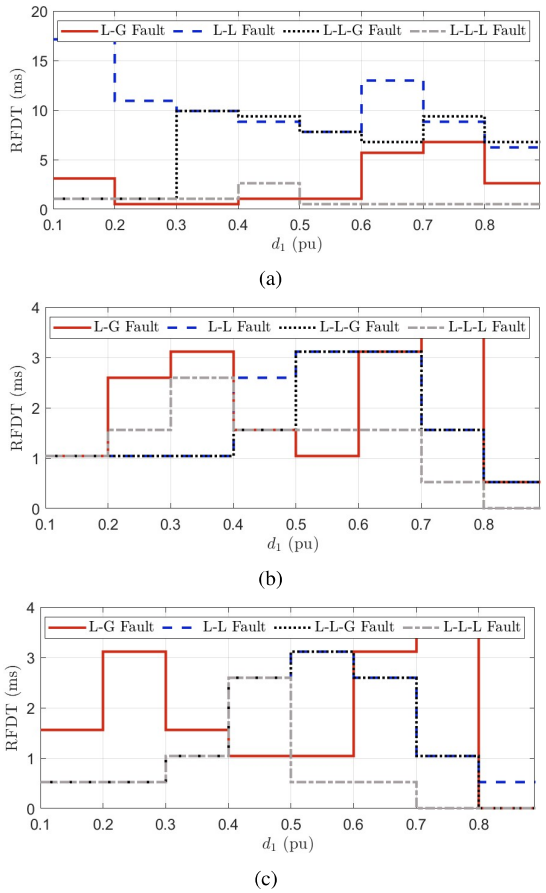

Fig. 7. Reducing the time for fault detection considering different types of polarization: (a) Self-polarized. (b) Cross-polarized. (c) Memory-polarized.

The fault events in the d_2 region are used to quantify the overreach and loss of directionality of the protection units installed at BUSA02 and BUSA03, respectively. Although many results were generated, due to space limitations, only the trip signals of the phase-to-ground (Z_{AG} and Z_{BG}) and phase-to-phase (Z_{AB}) protection units during $(A-B-G)$ faults type were evaluated, with the protection units being equipped with mho characteristic memory-polarized, because it is the most modern polarization technique [37]. The results obtained for the foregoing studies are presented in Figs. 8 and 9. It can be seen that protection units processing FCDFT estimated phasors may act improperly due to overreach or loss of directionality. On the other hand, units equipped with FCDFTC acted assertively in all cases presented.

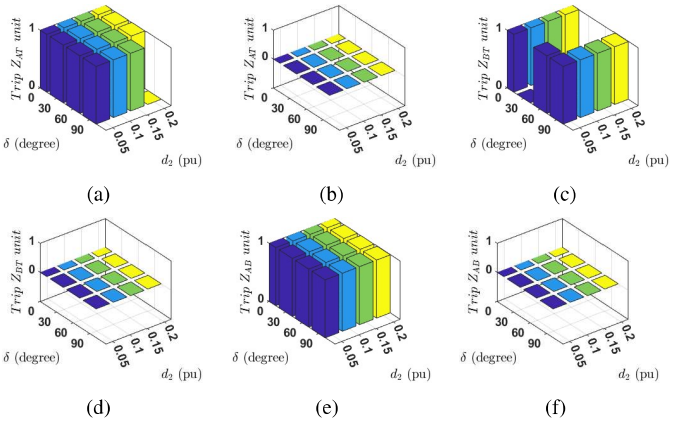

Fig. 8. Trip signals from protection units installed at BUSA02: (a) Z_{AT} unit with FCDFT. (b) Z_{AT} with FCDFTC. (c) Z_{BT} with FCDFT. (d) Z_{BT} with FCDFTC. (e) Z_{AB} with FCDFT. (f) Z_{AB} with FCDFTC.

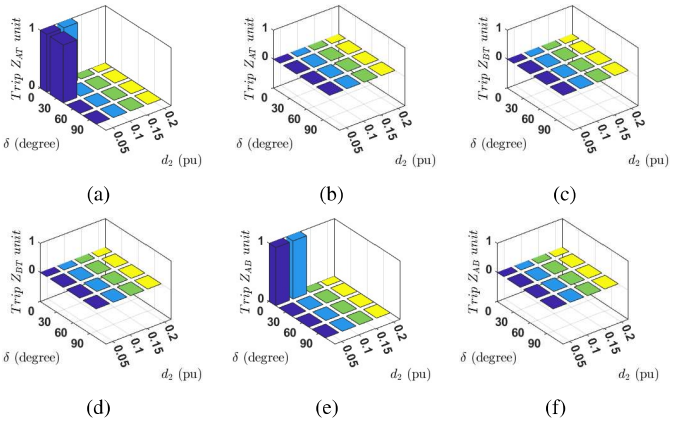

Fig. 9. Trip signals from protection units installed at BUSA03: (a) Z_{AT} unit with FCDFT. (b) Z_{AT} with FCDFTC. (c) Z_{BT} with FCDFT. (d) Z_{BT} with FCDFTC. (e) Z_{AB} with FCDFT. (f) Z_{AB} with FCDFTC.

V. CONCLUSION

Time domain correction methods for CCVT transients have practical implementation limitations since they must be embedded in IEDs during the manufacturing process or require a dedicated digital signal processor since users are not allowed to embed digital filters in IEDs and PMUs before the phase estimation process. In this paper, the

mathematical demonstration that the method developed by the authors for time domain sample correction of the secondary voltage of CCVTs can also be used to correct samples of the respective voltage phase. Since it is the same digital filter, the characteristics of independence of the measurement transformer topologies, knowledge of its parameters, and the nature of the power system are maintained, because only the frequency response of the equipment in the range between 10 and 60 Hz is used for the filter design. Using three different types of phasor estimation algorithms and four CCVT topologies, it was verified that the phase correction method eliminates the low-frequency oscillations caused by the sudden change of the voltage at the primary, providing more assertive phases to the protection and control algorithms during transient operating conditions.

REFERENCES

[1] B. Kasztenny, D. Sharples, V. Asaro, and M. Pozzuoli, "Distance Relays and Capacitive Voltage Transformers-Balancing Speed and Transient Overreach," in *53th Annual Conference for Protective Relay Engineers*, College station, Texas, USA, April 2000.

[2] D. Finney, Z. Zhang, and J. Cardenas, "Ultra Fast Distance Protetion," *Proceedings of the 10th International Conference on Developments in Power System Protection, Manchester, United Kingdom*, March 2010.

[3] G. A. Franklin and R. Horton, "Determining Distance Relay Zone-1 Reach Settings to Prevent CCVT Transient Overreach," *proceedings of IEEE, Southeastcon*, March 2011.

[4] C. Venkatesh and K. S. Swarup, "Performance Assessment of Distance Protection Fed by Capacitor Voltage Transformer with Electronic Ferro-resonance Suppression Circuit," *Electric Power Systems Research*, vol. 112, pp. 12 – 19, 2014.

[5] S. Gray, D. Haas, and R. McDaniel, "CCVT Failures and Their Effects on Distance Relays," in *71st Annual Conference for Protective Relay Engineers (CPRE)*, 2018, pp. 1–13.

[6] E. P. Machado, D. Fernandes Jr., , and W. L. A. Neves, "Tuning CCVT Frequency Response Data for Improvement of Numerical Distance Protection," *IEEE Transaction on Power Delivery*, vol. 33, no. 3, pp. 1062–1070, June 2018.

[7] R. Ferrero, P. A. Pegoraro, and S. Toscani, "Impact of Capacitor Voltage Transformers on Phasor Measurement Units Dynamic Performance," in *2018 IEEE 9th International Workshop on Applied Measurements for Power Systems (AMPS)*, 2018, pp. 1–6.

[8] S. S. K. Madahi, H. A. Abyaneh, C. A. Nucci, and M. Parpaei, "A New DFT-Based Frequency Estimation Algorithm for Protection Devices Under Normal and Fault Conditions," *International Journal of Electrical Power & Energy Systems*, vol. 142, p. 108276, 2022.

[9] Y. Liang, Z. Zhang, H. Li, J. Ding, G. Wang, and L. Chen, "A Robust and Accurate Discrete Fourier Transform-Based Phasor Estimation Method for Frequency Domain Fault Location of Power Transmission Lines," *IET Generation, Transmission & Distribution*, vol. 16, no. 10, pp. 1990–2002, 2022.

[10] S. Afrandideh and F. Haghjoo, "A DFT-Based Phasor Estimation Method Robust to Primary and Secondary Decaying DC Components," *Electric Power Systems Research*, vol. 208, p. 107907, 2022.

[11] H. Yu, Z. Jin, H. Zhang, and V. Terzija, "A Phasor Estimation Algorithm Robust to Decaying DC Component," *IEEE Transactions on Power Delivery*, vol. 37, no. 2, pp. 860–870, 2022.

[12] K. M. Silva and F. A. O. Nascimento, "Modified DFT-Based Phasor Estimation Algorithms for Numerical Relaying Applications," *IEEE Transactions on Power Delivery*, vol. 33, no. 3, pp. 1165–1173, 2018.

[13] B. Jafarpisheh, S. M. Madani, and F. Parvaresh, "Phasor Estimation Algorithm Based on Complex Frequency Filters for Digital Relaying," *IEEE Transactions on Instrumentation and Measurement*, vol. 67, no. 3, pp. 582–592, 2018.

[14] J. K. Hwang and C. S. Lee, "Fault Current Phasor Estimation Below One Cycle Using Fourier Analysis of Decaying DC Component," *IEEE Transactions on Power Delivery*, vol. 37, no. 5, pp. 3657–3668, 2022.

[15] E. Pajuelo, G. Ramakrishna, and M. Sachdev, "Strengths an Limitations of a New Phasor Estimation Technique to Reduce the CCVT Impact in Distance Protection," *Electric Power Systems Research*, vol. 80, no. 4, p. 417–425, 2010.

[16] F. B. Ajaei, M. Sanaye-Pasand, M. Davarpanah, A. Rezaei-Zare, and R. Iravani, "Mitigating the Impacts of CCVT Subsidence Transients on the Distance Relay," *IEEE Transactions on Power Delivery*, vol. 27, no. 2, pp. 497 –505, April 2012.

[17] C.-S. Yu, L.-R. Chang, and C.-J. Chou, "Line Voltage Phasor Reconstrutuction on Capacitive Voltage Transformers Using Dynamic Phasor Approach," *Journal of the Chinese Institute of Engineers*, 2015.

[18] H. B. Siguerdidjane, J. Gaonach, and N. L. Rohellec, "Applications of Digital Power Simulators: Advantages," *IEEE Transactions on Power Delivery*, vol. 12, no. 3, pp. 1137–1142, July 1997.

[19] J. Izykowski, B. Kasztenny, E. Rosolowski, M. M. Saha, and B. Hillstrom, "Dynamic Compensation of Capacitive Voltage Transformers," *IEEE Transactions on Power Delivery*, vol. 13, no. 1, pp. 116–122, January 1998.

[20] M. M. Saha, J. Izykowski, M. Lukowicz, and E. Rosolowski, "Application of ann Methods for Instrument Transformer Correction in Transmission Line Protection," in *Developments in Power System Protection*. IEE, 2001, pp. 303–306.

[21] S. M. Saleh, E. M. Abould-Zahab, E. T. Eldin, D. K. Ibrahim, and M. I. Gilany, "Neural Network-Based Technique Used for Recovery the CCVT Primary Signal," *Power & Energy Society General Meeting*, 2009.

[22] H. K. Zadeh and Z. Li, "Development and Hardware Implementation of a Reliable Protective Relay Data Acquisition System," *International Journal of Electrical Power & Energy Systems*, vol. 44, no. 1, pp. 495 – 505, 2013.

[23] M. Wen, D. Chen, and X. Yin, "Equal Transfer Processes-Based Distance Protection of EHV Transmission Lines," *International Journal of Electrical Power & Energy Systems*, vol. 52, no. 0, pp. 81 – 86, 2013.

[24] Y. Chen, M. Wen, Z. Wang, X. Yin, J. Peng, and R. Zhang, "An Improved Numerical Distance Relay Based on CCCVT Transient Characteristic Matching," *International Journal of Electrical Power & Energy Systems*, vol. 122, p. 106146, 2020.

[25] A. Ameli, M. Ghafouri, M. M. A. Salama, and E. F. El-Saadany, "An Auxiliary Framework to Mitigate Measurement Inaccuracies Caused by Capacitive Voltage Transformers," *IEEE Transactions on Instrumentation and Measurement*, vol. 71, pp. 1–11, 2022.

[26] M. Tajdinian, M. Allahbakhshi, A. R. Seifi, M. Z. Jahromi, and D. Behi, "Auxiliary Prony-Based Algorithm for Performance Improvement of DFT Phasor Estimator Against Transient of CCVT," *IET Science, Measurement & Technology*, vol. 13, pp. 708–714, July 2019.

[27] L. Kojovic, M. Kezunovic, V. Skendzic, C. W. Fromen, and D. R. Sevcik, "A New Method for the CCVT Performance Analysis Using Field Measurements, Signal Processing and EMTP Modeling," *IEEE Transactions on Power Delivery*, vol. 9, no. 4, pp. 1907–1915, October 1994.

[28] D. Fernandes, W. L. A. Neves, and J. C. A. Vasconcelos, "Coupling Capacitor Voltage Transformer: A Model for Electromagnetic Transient Studies," *Electric Power Systems Research*, vol. 77, no. 2, pp. 125–134, 2007.

[29] IEEE POWER SYSTEM RELAYING COMMITTEE, "EMTP Reference Models for Transmission Line Relay Testing," *IEEE PES/PSRC Report*, 2004.

[30] E. Pajuelo, G. Ramakrishna, and M. Sachdev, "Phasor Estimation Technique to Reduce the Impact of Coupling Capacitor Voltage Transformer Transients," *IET Generation, Transmission & Distribution*, vol. 2, no. 4, p. 588–599, 2008.

[31] A. T. Johns and S. K. Salman, *Digital Protection for Power Systems*, ser. IEE Power Series 15. Herts, United Kingdom: Peter Peregrinus Ltd., 1995.

[32] E. Schweitzer and D. Hou, "Filtering for Protective Relays," in *IEEE WESCANEX 93 Communications, Computers and Power in the Modern Environment - Conference Proceedings*, 1993, pp. 15–23.

[33] D. G. Hart, D. Novosel, and R. A. Smith, "Modified Cosine Filters," Patent, Nov. 2000.

[34] J. Proakis and D. G. Manolakis, *Digital Signal Processing: Principles, Algorithms, and Applications*. New Delhi: Prentice Hall, 2006.

[35] K. M. C. Dantas, E. P. Machado, W. L. A. Neves, and L. C. A. Fonseca, "Recursive Digital Filters Design to Compensate CVT Frequency Response: An Application for Transmission Line Controlled Switching," in *International Conference on Power Systems Transients (IPST)*, Cavtat, Croatia, Jun. 2015.

[36] D. Barros, W. L. A. Neves, and K. C. Dantas, "Controlled Switching of Series Compensated Transmission Lines: Challenges and Solutions," *IEEE Transaction on Power Delivery*, 2019.

[37] G. Ziegler, *Numerical Distance Protection: Principles and Applications*, 3rd ed., Siemens, Ed. Berlin, Germany: Siemens, 2008.